

## Theory of absorption in doping superlattices

Gottfried H. Döhler\* and Peter Paul Ruden†

Max-Planck Institut für Festkörperforschung, Heisenbergstrasse 1, D-7000 Stuttgart 80,  
Federal Republic of Germany

(Received 9 April 1984)

The absorption due to transitions between valence and conduction subbands in doping superlattices is calculated analytically and numerically. Results for various materials and design parameters of the superlattice configuration are presented for illustration. It is found that with an appropriate choice of design parameters the absorption coefficient exhibits a pronounced steplike structure for photon energies less than the band gap of the host material. The absorption of a given specimen is strongly tunable by external fields, by carrier injection, and by the generation of carriers due to the absorption process itself. At fixed photon energy, large-amplitude oscillations of the absorption coefficient as a function of both the external electric field and the induced carrier concentration are predicted. The limitations of our approach, and consequences of our results for interesting applications, are discussed briefly.

### I. INTRODUCTION

Doping (*n-i-p-i*) superlattices are a periodic array of *n*- and *p*-type doped layers which may be separated by undoped (*i*-) layers of the same semiconductor material. They represent a new class of synthetic semiconductors.<sup>1-4</sup> The most striking features by which they differ from their compositional counterparts<sup>5,6</sup> (e.g., GaAs-Al<sub>x</sub>Ga<sub>1-x</sub>As or InAs-GaSb superlattices), and from any homogeneous bulk semiconductor, is the strong tunability of their electronic structure and, consequently, of the resulting electrical and optical properties.<sup>7-13</sup> This tunability originates from an efficient spatial separation of electrons and holes, which is induced by the space-charge potential of the impurities. In addition to the tunability, i.e., the possibility of modulating the properties of a given specimen by applying external potentials<sup>8,12</sup> or light radiation,<sup>7,9,11,13</sup> the *n-i-p-i* systems exhibit an extreme flexibility with respect to the tailoring of their electronic structure. Any semiconductor, which can be *n* and *p* doped, can be used as host material for the *n-i-p-i* structure, in contrast to the compositional superlattices, where the requirement of lattice matching severely restricts the choice of materials. Furthermore, any value of the effective band gap  $E_g^{\text{eff},0}$  of the *n-i-p-i* crystal in the ground state that is smaller than the gap of the host material,  $E_g^0$ , can be generated by an appropriate choice of the design parameters, i.e., the doping concentration and the thickness of the layers. Similarly, the efficiency of the spatial separation of electrons and holes depends on the choice of the design parameters.<sup>10</sup> Finally, the two-dimensional subband structure can be tailored independently for electrons and holes, again due to their spatial separation.<sup>14</sup>

During the last few years intensive experimental studies on GaAs *n-i-p-i* crystals, grown by molecular-beam epitaxy (MBE),<sup>15</sup> have confirmed a large number of properties which were predicted in theoretical investigations, started by one of us (G.H.D.) more than a decade ago.<sup>1,2</sup> Simultaneously, the theory has been worked out in more

detail.<sup>14,16</sup> The tunable optical absorption which will be the subject of the present paper has also been studied theoretically and experimentally in a previous investigation.<sup>11</sup> The superlattice period in that particular case was chosen to be rather large, such that a theoretical description in terms of a semiclassical treatment (spatially modulated internal Franz-Keldysh effect) was appropriate. Good agreement between measured and calculated absorption coefficients was found for the ground state as well as for their tunability by optical excitation.

The purpose of the present paper is a more rigorous theoretical treatment of the absorption processes, taking into account the real two-dimensional subband structure. We will see that this more sophisticated treatment yields interesting new results. The two-dimensional subband structure leads to pronounced steps in the absorption coefficient  $\alpha^{n-i-p-i}(\omega)$  for photon energies  $\hbar\omega$  corresponding to transitions between the edges of the electron and hole subbands. Similarly, the absorption coefficient for a fixed photon energy exhibits an oscillatory behavior as a function of excitation level or external field. The variation of the excitation level, which is tantamount to a variation of the effective band gap, can be accomplished by various means, among them population changes induced by the absorbed probe light itself, light of different photon energy, and/or different direction and/or polarization, and, in addition, by electrical bias applied via selective electrodes. These changes of the absorption coefficient also include the change of its sign, i.e., the transition from absorption to amplification for a fixed photon energy. The specific features of *n-i-p-i* crystals allow for such a transition at unusually low excitation intensities and within a very wide photon-energy range. Apart from the changes of the absorption coefficient which are of particular interest for the generation, modulation, and amplification of light signals, the above-mentioned self-induced changes yield intensity-dependent absorption coefficients and refractive indices. As a consequence, it turns out that *n-i-p-i* crystals represent a promising basic material for devices based on

optical nonlinearity, such as bistable or multistable optical switches.<sup>17</sup>

In Sec. II of this paper we calculate analytically the absorption coefficient in the ground state for *n-i-p-i* crystals with a set of design parameters which leads to a particularly simple electronic structure. The analytical approach has the advantage of making transparent the relationship between absorption coefficient and design and materials parameters of the *n-i-p-i* superlattice. It also allows us to discuss the effects of external fields.

In Sec. III the absorption coefficient under external electric fields and in the excited state will be considered. We will treat analytically the former case and present numerical results obtained from self-consistent calculations of the electronic structure<sup>14</sup> for the excited state. These examples will demonstrate the strong tunability of the absorption coefficient as a function of external fields and of the excitation level. In our concluding remarks we will summarize our present results and we will critically review the approximations made and consider their consequences.

## II. ABSORPTION IN THE GROUND STATE

We consider a compensated *n-i-p-i* crystal with uniformly doped *n*- and *p*-type layers of thickness  $d_n$  and  $d_p$ , respectively, and doping concentrations  $n_D$  and  $n_A$ , respectively. The condition for compensation, i.e., the absence of free carriers in the ground state, reduces to

$$n_D d_n = n_A d_p \quad (1)$$

in this simple case.

The periodic space-charge potential of the ionized impurities is composed of parabolic segments and reads

$$v_0(z) = \begin{cases} (2\pi e^2 n_D / \kappa_0) z^2, & |z| \leq d_n/2 \\ 2V_0 - (2\pi e^2 n_A / \kappa_0) (|z| - d/2)^2, & (d - d_p)/2 < |z| \leq d/2 \end{cases} \quad (2)$$

for the zeroth period. The static dielectric constant is  $\kappa_0$  and  $e$  is the elementary charge. The potential amplitude  $V_0$  is given by

$$2V_0 = (2\pi e^2 / \kappa_0) [n_D (d_n/2)^2 + n_A (d_p/2)^2]. \quad (3)$$

This superlattice potential is superposed on the crystal potential of the host semiconductor. In Fig. 1 the real-space band scheme with the lower conduction-band and upper valence-band edge modulated by the superlattice potential is shown. The motion of the charge carriers in the  $z$  direction is quantized by the steep space-charge potential  $v_0(z)$ . The electrons in the lowest discrete energy levels  $E_{c,\mu}$  and holes in the uppermost valence-band states,  $E_{v,\nu}$  are defined by the respective parabolic parts of the potential. The eigenvalues are therefore harmonic-oscillator energies

$$E_{c,\mu}^{(i)} = E_g^0 - 2V_0 + \hbar\omega_c^{(i)}(\mu + \frac{1}{2}), \quad \mu = 0, 1, 2, \dots \quad (4)$$

and

$$E_{v,\nu}^{(j)} = -\hbar\omega_v^{(j)}(\nu + \frac{1}{2}), \quad \nu = 0, 1, 2, \dots \quad (5)$$

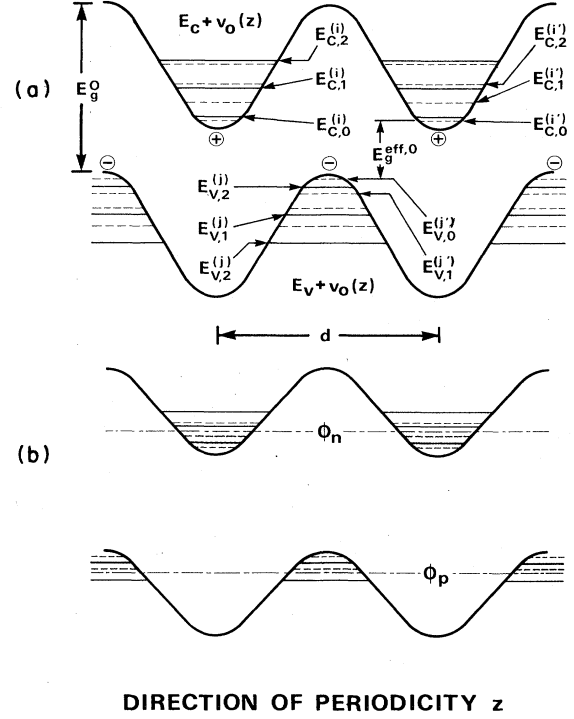


FIG. 1. Schematic real-space energy diagram of a compensated *n-i-p-i* crystal. The conduction- and valence-band edges are modulated by the space-charge potential of the ionized impurities (indicated by + and - signs for donors and acceptors, respectively). The dashed and solid horizontal lines close to the (real-space) conduction- and valence-band extrema correspond to the subband edges of different subband systems,  $E_{c,\mu}^{(i)}$  and  $E_{v,\nu}^{(j)}$ , derived from different conduction and valence bands ( $i$ ) and ( $j$ ), respectively. (a) shows the ground state of an *n-i-p-i* crystal, and (b) shows an excited state with carriers in the subbands, reduced subband spacing, reduced band modulation, and different quasi Fermi levels for electrons and holes.

within the effective-mass approximation (EMA). The harmonic-oscillator approximation is quite accurate for

$$(\hbar\omega_c^{(i)}(\mu + \frac{1}{2}), \hbar\omega_v^{(j)}(\nu + \frac{1}{2})) \gtrsim V_0, \quad (6)$$

to the extent that deviations of  $v_0(z)$  from parabolas influence the energy eigenvalues. For the validity of the EMA, however, the more restrictive condition

$$(\hbar\omega_c^{(i)}(\mu + \frac{1}{2}), \hbar\omega_v^{(j)}(\nu + \frac{1}{2})) \ll E_g^0 \quad (7)$$

must be fulfilled. The error introduced by neglecting deviations from the EMA is not serious as long as the deviations between the exact and EMA values are substantially smaller than the oscillator level spacing, e.g.,

$$|(E_{c,\mu}^{(i)})^{\text{exact}} - (E_{c,\mu}^{(i)})^{\text{EMA}}| \gtrsim 0.2\hbar\omega_c^{(i)}. \quad (8)$$

We have introduced the superscripts ( $i$ ) and ( $j$ ) in Eqs. (4) and (5) in order to take into account anisotropic and/or degenerate bands in realistic crystals. In the case of semiconductors with GaAs band structure, the conduction band is nearly isotropic and nondegenerate with an effective mass  $m_c$ . Therefore, we can omit the superscript; we obtain

$$\omega_c = [4\pi e^2 n_D / (\kappa_0 m_c)]^{1/2} \text{ for GaAs structures.} \quad (9)$$

For the two uppermost valence bands, the heavy-hole (HH) and the light-hole (LH) bands, we obtain, for tetrahedrally coordinated semiconductors,

$$\omega_v^{\text{HH}} = [4\pi e^2 n_A / (\kappa_0 m_{\text{HH}})]^{1/2}$$

and (10)

$$\omega_v^{\text{LH}} = [4\pi e^2 n_A / (\kappa_0 m_{\text{LH}})]^{1/2}.$$

Strictly speaking, we must take into account the anisotropy of the valence bands (particularly for the HH band). Therefore, we must use the appropriate components of the effective-mass tensor,  $m_{\text{HH},z}$  and  $m_{\text{LH},z}$ , in Eq. (10), which correspond to  $m_{\text{HH}}^{(100)}$  and  $m_{\text{LH}}^{(100)}$  if the  $z$  direction of the superstructure coincides with the (100) symmetry direction of the host-crystal lattice. We also note that the different bands of the host crystal interact because of the

potential  $v_0(z)$ . The consequences of this interband coupling are probably always unimportant for our present problem and will be neglected in the following.

If the host crystal exhibits a many-valley band structure (Si, Ge, or GaP, but also IV-VI compounds such as PbTe, for example), we must take into account the anisotropy of the energy bands. The effective masses in Eqs. (9) and (10) must be replaced by the appropriate values  $m_z$ , depending on the orientation of the superlattice direction with respect to the crystal symmetry axes. The solution of the Schrödinger equation and the values of  $m_z$  in terms of the longitudinal and transverse masses  $m_l$  and  $m_t$  have been calculated by Stern and Howard<sup>18</sup> for the symmetry directions (100), (110), and (111). We give here only the results for a IV-VI compound with superlattice orientation along the (111) direction. These compounds have conduction- and valence-band edges at the  $L$  points.<sup>19</sup> Equations (9) and (10) now read, for ( $a$ )-type valleys,

$$\omega_c^{(1)} = [4\pi e^2 n_D / (\kappa_0 m_{cl})]^{1/2}, \quad \omega_v^{(a)} = [4\pi e^2 n_A / (\kappa_0 m_{vl})]^{1/2} \quad (11)$$

and, for ( $b$ )-type valleys,

$$\omega_c^{(b)} = \{4\pi e^2 n_D / [\kappa_0 9 m_{ct} m_{cl} / (m_{ct} + 8m_{cl})]\}^{1/2}, \quad \omega_v^{(b)} = \{4\pi e^2 n_A / [\kappa_0 9 m_{vt} m_{vl} / (m_{vt} + 8m_{vl})]\}^{1/2}, \quad (12)$$

where we have followed the convention that the valley whose symmetry axis coincides with the direction of symmetry breaking is designated as ( $a$ ) type, and the other three degenerate valleys as ( $b$ ) type.

The energies  $E_{c,\mu}^{(i)}$  and  $E_{v,\nu}^{(j)}$  form the edges of the subbands with energies  $\epsilon_{c,\mu}^{(i)}(\vec{k}_{\parallel})$  and  $\epsilon_{v,\nu}^{(j)}(\vec{k}_{\parallel})$  given by

$$\epsilon_{c,\mu}^{(i)}(\vec{k}_{\parallel}) = E_{c,\mu}^{(i)} + \hbar^2 \sum_{l,m} (k_l - k_{0,l}^{(i)})(k_m - k_{0,m}^{(i)}) [(m_c^{(i)})^{-1}]_{l,m}, \quad (13)$$

$$\epsilon_{v,\nu}^{(j)}(\vec{k}_{\parallel}) = E_{v,\nu}^{(j)} - \hbar^2 \sum_{l,m} (k_l - k_{0,l}^{(j)})(k_m - k_{0,m}^{(j)}) [(m_v^{(j)})^{-1}]_{l,m}, \quad (14)$$

where  $[(m_c^{(i)})^{-1}]_{l,m}$  and  $[(m_v^{(j)})^{-1}]_{l,m}$  are the ( $l,m$ ) components of the reciprocal effective-mass tensor for the  $\vec{k}_{\parallel} = (k_x, k_y)$  direction. The  $\vec{k}_{0(j)}$  are the wave vectors of the band extrema.<sup>6</sup> The two-dimensional densities of states per subband,  $N_{c,\mu}^{(i)}(\epsilon)$  and  $N_{v,\nu}^{(j)}(\epsilon)$ , again in the EMA, are<sup>20</sup>

$$N_{c,\mu}(\epsilon) = (m_c / \pi \hbar^2) \Theta(\epsilon - E_{c,\mu}), \quad (15)$$

for GaAs structure,

$$N_{v,\nu}^{\text{HH}}(\epsilon) = (m_{\text{HH}} / \pi \hbar^2) \Theta(E_{v,\nu}^{\text{HH}} - \epsilon), \quad N_{v,\nu}^{\text{LH}}(\epsilon) = (m_{\text{LH}} / \pi \hbar^2) \Theta(E_{v,\nu}^{\text{LH}} - \epsilon), \quad (16)$$

for tetrahedrally coordinated semiconductors,

$$N_{c,\mu}^{(a)}(\epsilon) = (m_{ct} / \pi \hbar^2) \Theta(\epsilon - E_{c,\mu}^{(a)}), \quad N_{v,\nu}^{(a)}(\epsilon) = (m_{vt} / \pi \hbar^2) \Theta(E_{v,\nu}^{(a)} - \epsilon), \quad (17)$$

for ( $a$ ) valleys, and

$$N_{c,\mu}^{(b)}(\epsilon) = 3(m_{c,\text{DOS}}^{(b)} / \pi \hbar^2) \Theta(\epsilon - E_{c,\mu}^{(b)}), \quad N_{v,\nu}^{(b)}(\epsilon) = 3(m_{v,\text{DOS}}^{(b)} / \pi \hbar^2) \Theta(E_{v,\nu}^{(b)} - \epsilon), \quad (18)$$

for ( $b$ ) valleys, where the two-dimensional density-of-states (DOS) masses for motion of carriers parallel to the layers in the ( $b$ ) valleys,  $m_{c,\text{DOS}}^{(b)}$  and  $m_{v,\text{DOS}}^{(b)}$ , are given by

$$m_{c,\text{DOS}}^{(b)} = [m_{ct}(m_{ct} + 8m_{cl})/9]^{1/2}, \quad m_{v,\text{DOS}}^{(b)} = [m_{vt}(m_{vt} + 8m_{vl})/9]^{1/2}. \quad (19)$$

We have neglected the finite bandwidth of the subbands with respect to propagation in the  $z$  direction. This is justified by the fact that this bandwidth, in general, is negligibly small for all the subbands participating in optical transitions which will be of interest in this paper. Similarly, it is sufficient to use the wave functions of isolated potential wells for the calculation of the dipole matrix elements for the optical transitions.

The wave function for the  $\mu$ th ( $i$ )-type conduction subband becomes, in the layer of index  $m$ , in the EMA,

$$\langle \vec{r} | c, (i), \mu, \vec{k}_{\parallel}, m \rangle \simeq e^{i\vec{k}_{\parallel} \cdot \vec{r}_{\parallel}} \frac{1}{\sqrt{S_{c,\mu}}} \epsilon_{c,\mu}^{(i)}(z - md) u_{c,\vec{k}_{0}^{(i)}}(\vec{r}) e^{ik_{0,z}^{(i)} z}, \quad (20)$$

and, for the  $\nu$ th ( $j$ )-type valence subband,

$$\langle \vec{r} | v, (j), \nu, \vec{k}_{||}, m \rangle \simeq e^{i\vec{k}_{||} \cdot \vec{r}} \xi_{v,\nu}^{(j)} [z - (m + \frac{1}{2})d] u_{v,\vec{k}_{||}}^{(j)}(\vec{r}) e^{ik_{0,z}^{(j)} z}, \quad (21)$$

where the  $u$ 's are the (host-) lattice-periodic parts of the respective Bloch functions at the conduction-band minima  $\vec{k}_0^{(i)}$  and valence-band maxima  $\vec{k}_0^{(j)}$ . The envelope wave functions  $\xi_{c,\mu}^{(i)}(z)$  and  $\xi_{v,\nu}^{(j)}(z)$  are harmonic-oscillator solutions within the approximations discussed at the beginning of this section. For  $-d/2 < z \leq d/2$ , we have

$$\xi_{c,\mu}^{(i)}(z) \simeq \pi^{-1/4} (\alpha_c^{(i)})^{-1/2} \exp[-z^2/2(\alpha_c^{(i)})^2] (\mu! 2^\mu)^{-1/2} H_\mu(z/\alpha_c^{(i)}) \quad (22)$$

and

$$\xi_{v,\nu}^{(j)}(z) \simeq \pi^{-1/4} (\alpha_v^{(j)})^{-1/2} \exp[-(d/2 - |z|)^2/2(\alpha_v^{(j)})^2] (\nu! 2^\nu)^{-1/2} H_\nu[(d/2 - |z|)/\alpha_v^{(j)}], \quad (23)$$

where the  $H_\lambda(\xi)$  are the Hermite polynomials,

$$H_0(\xi) = 1, \quad H_1(\xi) = 2\xi, \quad (24)$$

$$H_2(\xi) = 4\xi^2 - 2, \quad H_3(\xi) = 8\xi^3 - 12\xi,$$

and

$$\alpha_c^{(i)} = (\hbar/m_{c,z} \omega_c^{(i)})^{1/2}, \quad (25)$$

$$\alpha_v^{(j)} = (\hbar/m_{v,z} \omega_v^{(j)})^{1/2}. \quad (26)$$

We have treated in some detail the relationship between the two-dimensional subband structure of the  $n$ - $i$ - $p$ - $i$  superlattice and the electronic structure of the host crystal because we will find that optical-interband-transition probabilities depend very sensitively on the specific subband system involved. We will exclude from our consideration the interesting case of absorption in  $n$ - $i$ - $p$ - $i$  systems made from a host material with an indirect gap in momentum space, such as Si, Ge, or GaP. For valleys which are projected onto the  $\Gamma$  point of the  $(k_x, k_y)$  plane, the vertical valence-band-to-conduction-band transitions are no longer strictly forbidden, which means that the crystal becomes a direct-gap semiconductor. A reasonably realistic treatment of this situation, however, would

lead beyond the scope of the present paper.

We now turn to the calculation of the absorption coefficient of an  $n$ - $i$ - $p$ - $i$  crystal in its ground state  $\alpha^{n-i-p-i}(\omega; E_g^{\text{eff},0})$ . Here,  $E_g^{\text{eff},0}$  stands for the effective band gap in the ground state, defined by (see Fig. 1)

$$E_g^{\text{eff},0} = E_g^0 - 2V_0 + \min_{i,j} (\hbar\omega_c^{(i)}/2 + \hbar\omega_v^{(j)}/2). \quad (27)$$

This energy represents the threshold photon energy for absorption. Excitonic effects are normally negligible in  $n$ - $i$ - $p$ - $i$  crystals because of the rather large average value of the electron-hole distance of  $d/2$ . The value of the absorption coefficient near  $E_g^{\text{eff},0}$  is always considerably smaller than typical bulk values because the interband dipole matrix elements

$$\langle c, (i), 0, \vec{k}_{||}, m | \vec{p} | v, (j), 0, \vec{k}_{||}, m \rangle$$

are small due to the spatial separation of the initial and final states. With increasing photon energy, transitions between subbands with higher indices  $\mu$  and  $\nu$  becomes energetically possible. The imaginary part of the dielectric function  $\epsilon_2^{n-i-p-i}(\omega_{\vec{\lambda}}; E_g^{\text{eff},0})$ , for photons  $\hbar\omega_{\vec{\lambda}}$  with polarization vector  $\vec{\lambda}$ , becomes

$$\epsilon_2^{n-i-p-i}(\omega_{\vec{\lambda}}; E_g^{\text{eff},0}) = \frac{4\pi^2 e^2}{A\alpha} \sum_{\mu,\nu, \vec{k}_{||}(i),(j)} \frac{2\hbar^2 |\langle c, (i), \mu, \vec{k}_{||}, m | \vec{p} \cdot \vec{\lambda} | v, (j), \nu, \vec{k}_{||}, m \rangle|^2}{m_0^2 [\epsilon_{c,\mu}^{(i)}(\vec{k}_{||}) - \epsilon_{v,\nu}^{(j)}(\vec{k}_{||})]^2} \delta(\epsilon_{c,\mu}^{(i)}(\vec{k}_{||}) - \epsilon_{v,\nu}^{(j)}(\vec{k}_{||}) - \hbar\omega_{\vec{\lambda}}). \quad (28)$$

The absorption coefficient  $\alpha^{n-i-p-i}(\omega_{\vec{\lambda}}; E_g^{\text{eff},0})$  is related to  $\epsilon_2^{n-i-p-i}(\omega_{\vec{\lambda}}; E_g^{\text{eff},0})$  by

$$\alpha(\omega) = \epsilon_2(\omega) \omega / [n_{\text{opt}}(\omega) c], \quad (29)$$

where  $n_{\text{opt}}(\omega)$  is the refractive index and  $c$  is the velocity of light.

Equation (28) will be evaluated for two simple examples. We take advantage of the fact that the two-dimensional subband structure for electrons and holes can be tailored independently. We choose the design parameters  $d_n$ ,  $d_p$ ,  $n_D$ , and  $n_A$  such that  $\omega_c^{(i)} = \omega_v^{(j)}$  for those subband systems which yield the major contributions to  $\epsilon_2^{n-i-p-i}(\omega_{\vec{\lambda}}; E_g^{\text{eff},0})$ . This requirement is fulfilled if

$$\frac{n_D}{n_A} = \frac{d_p}{d_n} = \begin{cases} m_c/m_{\text{LH}}, & \text{for GaAs structure,} \\ m_{c,z}^{(b)}/m_{v,z}^{(b)}, & \text{for IV-VI compounds,} \end{cases} \quad (30)$$

depending on the band structure of the host crystal.

This particular choice of design parameters has two advantages. The  $(i, j)$  contribution to the absorption increases at

equidistant photon energy intervals,

$$\hbar\omega_0 = \hbar\omega_c^{(i)} = \hbar\omega_v^{(j)}, \quad (32)$$

and the analytical evaluation of (28) with the wave functions given by Eqs. (22)–(24) yields rather accurate results. We find

$$|\langle c, (i), \mu, \vec{k}_{||} | \vec{p} \cdot \vec{\lambda} | v, (j), \nu, \vec{k}_{||} \rangle|^2 \simeq 2 |\langle c, (i), \vec{k}_0^{(i)} | \vec{p} \cdot \vec{\lambda} | v, (j), \vec{k}_0^{(j)} \rangle|^2 \left| \int dz \xi_{c,\mu}^{(i)}(z) \xi_{v,\nu}^{(j)}(d/2 - |z|) \right|^2, \quad (33)$$

with

$$\left| \int \xi_{c,\mu}^{(i)}(z) \xi_{v,\nu}^{(j)}(d/2 - |z|) dz \right|^2 = \exp\{-(d/2)^2 / [(\alpha_c^{(i)})^2 + (\alpha_v^{(j)})^2]\} I_{\mu,\nu}^{(i)(j)}. \quad (34)$$

Equation (33) contains only a contribution of  $\vec{p}$  operating on the Bloch states, but no contribution of  $\vec{p}$  acting on the envelope functions because of the orthogonality of Bloch states belonging to different bands. The exponent in Eq. (34) can be rewritten as

$$\frac{(d/2)^2}{(\alpha_c^{(i)})^2 + (\alpha_v^{(j)})^2} = 2 \frac{2V_0(d_n + d_p)}{\hbar\omega_c^{(i)} d_n + \hbar\omega_v^{(j)} d_p}, \quad (35)$$

and reduces to

$$\frac{(d/2)^2}{(\alpha_c^{(i)})^2 + (\alpha_v^{(j)})^2} = 2 \frac{2V_0}{\hbar\omega_c^{(j)}} \quad (36)$$

for transitions between those bands for which  $\omega_c^{(i)} = \omega_v^{(j)}$ . The integrand in the expression

$$I_{\mu,\nu}^{(i)(j)} = \exp\{(d/2)^2 / [(\alpha_c^{(i)})^2 + (\alpha_v^{(j)})^2]\} \left| \int dz \xi_{c,\mu}^{(i)}(z) \xi_{v,\nu}^{(j)}(d/2 - |z|) \right|^2 \quad (37)$$

has its maximum near the boundary between the  $n$ - and  $p$ -doped regions for the subband wave functions under consideration. This is not the case for transitions between the electron and heavy-hole subbands. Therefore the analytical results are less accurate for the latter case because the wave functions differ significantly from harmonic-oscillator solutions in the region where the integrand is large.

For the lowest subbands, one finds

$$\begin{aligned} I_{0,0}^{(i)(j)} &= 2\alpha_c^{(i)} \alpha_v^{(j)} / [(\alpha_c^{(i)})^2 + (\alpha_v^{(j)})^2], \\ I_{1,0}^{(i)(j)} &= I_{0,0}^{(i)(j)} (\alpha_c^{(i)} d)^2 / \{2[(\alpha_c^{(i)})^2 + (\alpha_v^{(j)})^2]\}^2, \\ I_{2,0}^{(i)(j)} &= I_{0,0}^{(i)(j)} (\alpha_c^{(i)})^4 / \{8[(\alpha_c^{(i)})^2 + (\alpha_v^{(j)})^2]\} \{d^2 / [(\alpha_c^{(i)})^2 + (\alpha_v^{(j)})^2] + 2(\alpha_v^{(j)})^2 / (\alpha_c^{(i)})^2 - 2\}^2, \\ I_{1,1}^{(i)(j)} &= I_{0,0}^{(i)(j)} (\alpha_c^{(i)} \alpha_v^{(j)})^2 / \{4[(\alpha_c^{(i)})^2 + (\alpha_v^{(j)})^2]\} \{d^2 / [(\alpha_c^{(i)})^2 + (\alpha_v^{(j)})^2] - 4\}^2, \\ I_{3,0}^{(i)(j)} &= I_{0,0}^{(i)(j)} (\alpha_c^{(i)} d)^2 / \{48[(\alpha_c^{(i)})^2 + (\alpha_v^{(j)})^2]\} \{(\alpha_c^{(i)} d)^2 / [(\alpha_c^{(i)})^2 + (\alpha_v^{(j)})^2] + 6[(\alpha_v^{(j)})^2 - (\alpha_c^{(i)})^2] / [(\alpha_c^{(i)})^2 + (\alpha_v^{(j)})^2]\}^2, \\ I_{2,1}^{(i)(j)} &= I_{0,0}^{(i)(j)} d \alpha_v^{(j)} / [(\alpha_c^{(i)})^2 + (\alpha_v^{(j)})^2]^2 \{4[(\alpha_c^{(i)})^2 + (\alpha_v^{(j)})^2]\} + [-2(\alpha_c^{(i)})^2 + (\alpha_v^{(j)})^2] / [(\alpha_c^{(i)})^2 + (\alpha_v^{(j)})^2] - \frac{1}{2}\}^2. \end{aligned} \quad (38)$$

(The integrals  $I_{0,1}^{(i)(j)}$ ,  $I_{0,2}^{(i)(j)}$ , and  $I_{0,3}^{(i)(j)}$  follow from the corresponding terms by interchanging  $\alpha_c^{(i)} \leftrightarrow \alpha_v^{(j)}$ .)

We note the following observations.

(1) The interband dipole matrix elements in  $n$ - $i$ - $p$ - $i$  crystals are reduced by an exponential factor

$$\exp\left[-\frac{4V_0(d_n + d_p)}{\hbar\omega_c^{(i)} d_n + \hbar\omega_v^{(j)} d_p}\right]$$

with respect to bulk transitions or those in heterostructure superlattices.

(2) The matrix elements depend strongly on the effective masses of the bands, as  $\omega_{c,v} \propto m_{c,v}^{-1/2}$ . Thus, for  $V_0 > (\hbar\omega_c^{(i)}, \hbar\omega_v^{(j)})$ , the heavy-hole-subband-to-conduction-subband transitions are negligible compared to the light-hole-subband-to-conduction-subband transitions in typical  $n$ - $i$ - $p$ - $i$  structures if the host crystal has GaAs-type band structure. For  $n_A = 4 \times 10^{18} \text{ cm}^{-3}$ ,

$n_D = (m_c / m_{LH}) n_A$ , and  $d = 40 \text{ nm}$ , we find

$$\begin{aligned} |\langle c, \mu=0, \vec{k}_{||}, m | \vec{p} \cdot \vec{\lambda} | v, \text{LH}, \nu=0, \vec{k}_{||}, m \rangle|^2 \\ \simeq 2 |\langle c, \vec{k} | \vec{p} \cdot \vec{\lambda} | v, \text{LH}, \vec{k} \rangle|^2 e^{-14} \end{aligned} \quad (39)$$

and

$$\begin{aligned} |\langle c, \mu=0, \vec{k}_{||}, m | \vec{p} \cdot \vec{\lambda} | v, \text{HH}, \nu=0, \vec{k}_{||}, m \rangle|^2 \\ \simeq 2 |\langle c, \vec{k} | \vec{p} \cdot \vec{\lambda} | v, \text{HH}, \vec{k} \rangle|^2 e^{-20}. \end{aligned} \quad (40)$$

Similarly, we find, for PbTe,  $n$ - $i$ - $p$ - $i$  structure with  $n_D = n_A = 2 \times 10^{18} \text{ cm}^{-3}$  and  $d_n = d_p = 90 \text{ nm}$ ,

$$\begin{aligned} |\langle c, (b), \mu=0, \vec{k}_{||}, m | \vec{p} \cdot \vec{\lambda} | v, (b), \nu=0, \vec{k}_{||}, m \rangle|^2 \\ = 2 |\langle c, (b), \vec{k} | \vec{p} \cdot \vec{\lambda} | v, (b), \vec{k} \rangle|^2 e^{-10}, \end{aligned} \quad (41)$$

whereas the corresponding matrix elements for transitions

between the (large-effective-mass) ( $a$ ) valleys are much smaller

$$|\langle c, (a), \mu=0, \vec{k}_{||}, m | \vec{p} \cdot \lambda | v, (a), \nu=0, \vec{k}_{||}, m \rangle|^2 \\ = 2 |\langle c, (a), \vec{k} | \vec{p} \cdot \vec{\lambda} | v, (a), \vec{k} \rangle|^2 e^{-35}. \quad (42)$$

Note, that ( $a$ )-to-( $b$ ) transitions are forbidden by the  $\vec{k}_{||}$ -selection rule.

(3) There is no ( $\mu, \nu$ ) selection or quasi selection rule because of the spatial shift between the initial- and the final-state harmonic-oscillator wave functions ("indirect gap in real space"<sup>3,4</sup>). This is in contrast to heterojunction superlattices with a direct gap in real space.

(4) The matrix elements increase rapidly with increasing subband indices, i.e., for transitions which become energetically allowed for higher photon energies the absorption is much larger.

(5) For a GaAs-type band structure we can use the Kane model to describe the cell periodic part of the Bloch functions.<sup>21</sup> For the light-hole band with an effective spin of  $+\frac{1}{2}$ , for instance, one has

$$u_{vk}^{(\text{LH})+} = a^{(\text{LH})}(k) |iS\beta\rangle + b^{(\text{LH})}(k) |(X - iY)\alpha\rangle > 2^{-1/2} \\ + c^{(\text{LH})}(k) |Z\beta\rangle, \quad (43)$$

where  $|S\rangle$ ,  $|X\rangle$ ,  $|Y\rangle$ , and  $|Z\rangle$  stand for wave functions of  $s$  and  $p$  symmetry, and  $\alpha$  and  $\beta$  are spinors. The  $k$ -dependent coefficients  $a^{(\text{LH})}(k)$ ,  $b^{(\text{LH})}(k)$ , and  $c^{(\text{LH})}(k)$  reduce, in the limit  $k \rightarrow 0$ , to

$$a^{(\text{LH})}(0)=0, \quad b^{(\text{LH})}(0)=3^{-1/2}, \quad c^{(\text{LH})}(0)=(\frac{2}{3})^{1/2}. \quad (44)$$

The conduction-band wave function is given by a similar linear combination. Its coefficients for  $k \rightarrow 0$  reduce to

$$a^{(c)}(0)=1, \quad b^{(c)}(0)=0, \quad c^{(c)}(0)=0. \quad (45)$$

This form of the wave functions has the following two interesting consequences for optical absorption in doping superlattices.

(a) The absorption coefficient will be polarization dependent since the momentum matrix elements  $p_x, p_y$  will, in general, not be equal to that of  $p_z$ . However, a factor-of-4 difference between polarization  $\lambda$  in the plane of the layers and perpendicular to it, which is expected from Eq. (44), i.e., from using the effective-mass approximation, will not be observed. Even for the lowest subband the superlattice potential will mix Bloch functions of appreciable  $k_z$  ( $\vec{k}$  vector along the superlattice axis). This mixing is not described by the (lowest-order) wave function of Eqs. (20) and (21). The superposition of Bloch states of different  $k_z$  causes the differences in the matrix elements to diminish even for states near the subband edges, i.e., states with zero transverse momentum  $\vec{k}_{\perp}$ .

(b) The form of the wave functions (43) implies the possibility of exciting electrons of only one spin direction from the light-mass valence into the conduction band by applying circularly polarized light which propagates along the superlattice axis. Large degrees of conduction-electron spin polarization should be obtainable by absorption near the subband edges in  $n$ - $i$ - $p$ - $i$  crystals due to the separation of light- and heavy-mass valence-bands (dispar-

TABLE I. Material parameters for GaAs, InAs, and PbTe, and one example of a set of doping superlattice parameters for each material.

$E_g^0$ (eV)	$\kappa_0$	$P_{(hmn)}^2$ (eV)	Material parameters ( $T=4$ K)				Example superlattice parameters																
			$\left[ \frac{m_{c,v}}{m_0} \right]_{(hmn)}$	$n_D$ ( $\text{cm}^{-3}$ )	$n_A$ ( $\text{cm}^{-3}$ )	$d_n$ (nm)	$d_p$ (nm)	$E_g^{\text{eff},0}$ (eV)	$\left[ \frac{m_{c,v}}{m_0} \right]_z$	$\left[ \frac{m_{c,v}}{m_0} \right]_{\text{DOS}}$	$\hbar\omega_{c,v}^{(i)}$ (meV)												
GaAs	1.52	12.5	c 0.067 LH 0.074 0.4 HH 0.8	$3.62 \times 10^{18}$	$4.00 \times 10^{18}$	21	19	1.02	0.067 0.074 0.4	0.067 0.074 0.47	76.9 76.9 33.1												
												InAs	0.42	15.2	c 0.023 LH 0.025 HH 0.4	$5.00 \times 10^{17}$	$5.43 \times 10^{17}$	50	46	0.090	0.023 0.025 0.4	0.023 0.025 0.4	44.2 44.2 11.1

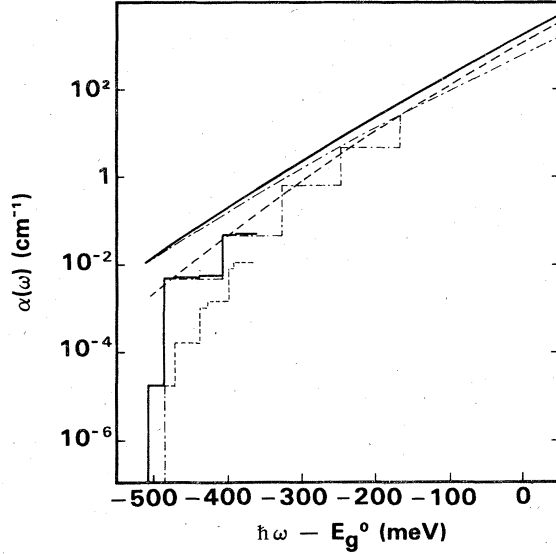


FIG. 2. Calculated absorption coefficient  $\alpha(\omega)$  for a GaAs  $n$ - $i$ - $p$ - $i$  crystal with  $n_A = 4 \times 10^{18}$ ,  $n_A = (m_{LH} m_c) n_D$ , and  $d = 40$  nm. Dashed lines depict the heavy-hole and the dashed-dotted lines the light-hole contributions, whereas the solid lines correspond to the sum of these contributions. The analytic calculation has only been performed for transitions with  $\mu, \nu \leq 3$ . The continuous curves show corresponding results of semiclassical calculations similar to those presented in Ref. 11.

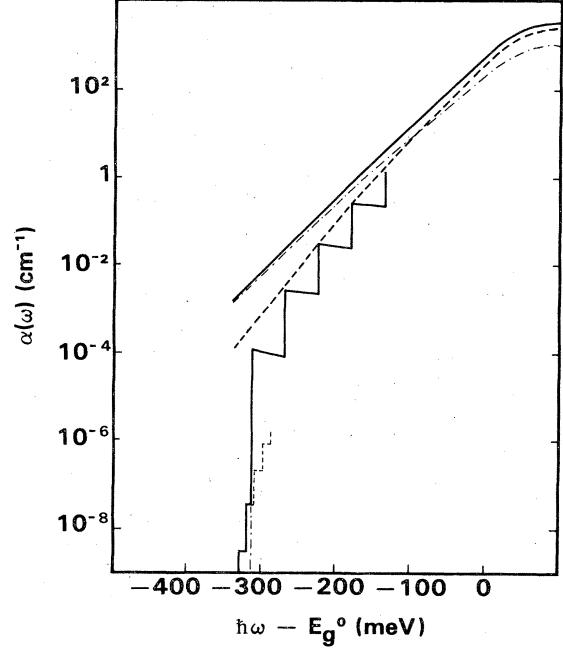


FIG. 3. Same as Fig. 2, but for an InAs  $n$ - $i$ - $p$ - $i$  crystal with  $n_D = 5 \times 10^{17} \text{ cm}^{-3}$  and  $d = 96$  nm. The difference between the heavy- and light-hole contributions is more pronounced than in the former case. In addition, the semiclassical description is found to overestimate considerably the absorption coefficient in this low-effective-band-gap example.

ity in the momentum matrix elements) and the imposition of a symmetry axis given by the direction of the built-in electric fields. This is particularly significant since the electron-hole scattering, which is thought to be the dominant spin-relaxation mechanism in GaAs at low carrier energies,<sup>22</sup> is much less effective in  $n$ - $i$ - $p$ - $i$  crystals than in bulk GaAs due to the large spatial separation of electrons and holes. Appropriate treatment of a surface perpendicular to the layers with cesium oxide, yielding a negative electron affinity,<sup>23</sup> may turn GaAs-doping superlattices

into a very efficient source of spin-polarized electrons.

The  $\vec{k}_{\parallel}$  summation in Eq. (28) yields two-dimensional interband densities of states,

$$N_{\mu\nu}^{(i)(j)}(\epsilon) = \{[(m_{c,\text{DOS}}^{(i)})^{-1} + (m_{v,\text{DOS}}^{(j)})^{-1}]^{-1} / \pi \hbar^2\} \times \Theta(\epsilon - E_{c,\mu}^{(i)} + E_{v,\nu}^{(j)}). \quad (46)$$

For our two cases under consideration the interband density-of-states masses in (46) are given by

$$(m_{c,\text{DOS}}^{(i)})^{-1} + (m_{v,\text{DOS}}^{(j)})^{-1} = \begin{cases} m_c^{-1} + m_{\text{HH}}^{-1} & m_c^{-1} + m_{\text{LH}}^{-1} \text{ for GaAs band structures,} \\ m_{ct}^{-1} + m_{vt}^{-1} & \text{for (a) valleys,} \\ 3[m_{ct}(m_{ct} + 8m_{cl})]^{-1/2} + 3[m_{vt}(m_{vt} + 8m_{vl})]^{-1/2} & \text{for (b) valleys.} \end{cases} \quad (47)$$

In both cases the absorption near the threshold photon energy

$$\hbar\omega^{\text{th}} = E_g^{\text{eff},0} \quad (48)$$

is due to the  $\nu=0$ -to- $\mu=0$  transition with the smallest matrix elements. Above the threshold for light-hole-band-to-conduction-band, or (b)-valley, transitions,

$$\hbar\omega^{\text{th}} = \tilde{E}_g^{\text{eff},0} = \begin{cases} E_{c,0} - E_{v,0}^{\text{LH}} & \text{for GaAs structures,} \\ E_{c,0}^{(b)} - E_{v,0}^{(b)} & \text{for IV-VI compounds,} \end{cases} \quad (49)$$

the latter contributions dominate the absorption coefficient. This is true, in particular, for the IV-VI compounds as the density-of-states factor is much larger for the (b) valleys, in addition to the larger matrix elements.

In Figs. 2 and 3 analytically calculated absorption coefficients for the ground state  $\alpha^{n-i-p-i}(\omega; E_g^{\text{eff},0})$  for GaAs and InAs  $n$ - $i$ - $p$ - $i$  crystals, respectively, are shown. The materials and design parameters are given in Table I. Also shown are the absorption curves which would be obtained from a semiclassical calculation as it was used in Ref. 11. Note that the in-

terband effective mass  $\mu_i$ , defined by Eq. (36) in Ref. 11, must be replaced by the appropriate quantities  $\mu_{i,z}$  in Eq. (34) and by  $\mu_{i,\text{DOS}}^{2/3}\mu_{i,z}^{1/3}$  in Eq. (33) if the bands are anisotropic. Here,  $\mu_{i,\text{DOS}}$  is identical with the expressions given in Eq. (47), and  $\mu_{i,z}$  is defined by

$$\mu_{i,z}^{-1} = \begin{cases} m_{c,l}^{-1} + m_{v,l}^{-1} & \text{for (a) valleys,} \\ (9m_{cl})^{-1} + (9m_{cl}/8)^{-1} + (9m_{vl})^{-1} + (9m_{vl}/8)^{-1} & \text{for (b) valleys.} \end{cases} \quad (50)$$

It is now quite obvious how we can tailor the absorption coefficient of an  $n$ - $i$ - $p$ - $i$  crystal by an appropriate choice of host material and design parameters  $n_D$ ,  $n_A$ , and  $d$ .

The absorption edge  $\hbar\omega^{\text{th}}$  shifts to lower values with increasing  $V_0$ , which, according to Eq. (3), is proportional to the doping concentration, the square of the superlattice period, and the inverse of the static dielectric constant. The width between the steps, with our particular choice of the subband distances  $\hbar\omega_c = \hbar\omega_{\text{LH}}$  or  $\hbar\omega_c^{(b)} = \hbar\omega_v^{(b)}$ , is proportional to the square root of the doping concentration, over the relevant effective mass and the inverse static dielectric constant, according to Eqs. (9)–(12). The average slope in the region  $\hbar\omega^{\text{th}} < \hbar\omega < E_g^0$ , where  $\ln\alpha^{n-i-p-i}(\omega)$  is staircase shaped, can easily be estimated from the semiclassical calculation. We find that the average slope is approximately proportional to the inverse maximum space-charge field  $F_{\text{max}}$ ,

$$F_{\text{max}} = 2\pi en_D d_n / \kappa_0, \quad (51)$$

and to the square root of the smallest reduced mass  $\mu_{i,z}$ . Thus,  $\ln\alpha^{n-i-p-i}(\omega)$  versus  $\omega$  becomes particularly flat in materials with small effective masses if the product

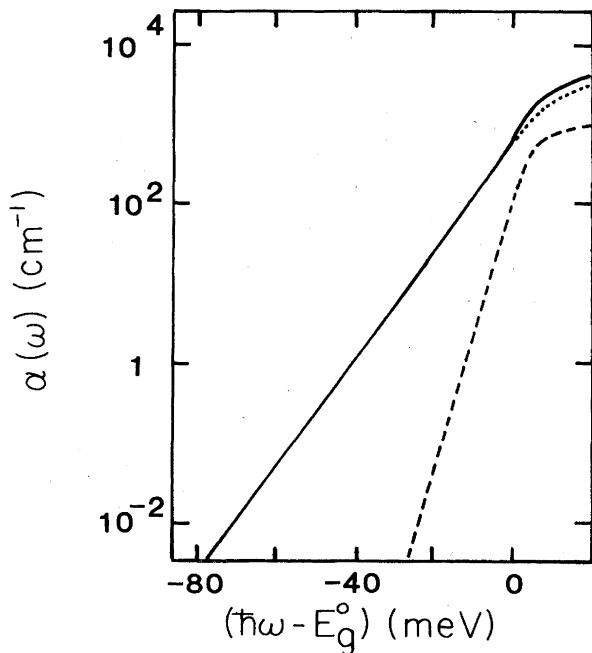


FIG. 4. Absorption coefficient of a PbTe doping superlattice with  $n_D = n_A = 10^{18} \text{ cm}^{-3}$  and  $d = 500 \text{ nm}$ . The dashed line represents the contribution of the (a) transitions. The contribution of the (b) transitions (dotted line) practically coincides with the total absorption coefficient (solid line) for photon energies smaller than  $E_g^0$ . The steplike structure is not shown due to the smallness of the subband spacing in this particular example.

$n_D d_n = n_A d_p$  is made large. Figure 4 shows the absorption coefficient of a PbTe  $n$ - $i$ - $p$ - $i$  crystal.

### III. TUNABLE ABSORPTION COEFFICIENT

The absorption coefficient of an  $n$ - $i$ - $p$ - $i$  crystal can be changed drastically by the application of external electric or magnetic fields or by varying the effective band gap  $E_g^{\text{eff}}$  through the injection or optical generation of electrons and holes. We defer the magnetoabsorption to a planned later publication and restrict ourselves to the modifications induced by an external electric field  $F_z$ , applied in the direction of periodicity (Sec. III A), and the variation of  $\alpha^{n-i-p-i}(\omega; E_g^{\text{eff},n})$  induced by variation of the effective band gap in the excited state (Sec. III B).

#### A. Absorption with external electric field

In Fig. 5 the band profiles  $\epsilon_c(z)$  and  $\epsilon_v(z)$  of an  $n$ - $i$ - $p$ - $i$  crystal with an external field  $F_z$  applied in the direction of periodicity are shown. Such a field can be induced by an external bias  $U_z$  applied between sandwich electrodes on the top and the bottom of the  $n$ - $i$ - $p$ - $i$  structure,

$$F_z = U_z / (N_{\text{sl}} d), \quad (52)$$

if the  $n$ - $i$ - $p$ - $i$  structure consists of  $N_{\text{sl}}$  periods.

The uniform field  $F_z$  does not affect the parabolic shape of the superlattice potential

$$v_F(z) = v_0(z) - eF_z z. \quad (53)$$

Therefore, the energetic separation between subbands of the same subband system,  $\hbar\omega^{(i)}$ , does not change either. The energetic and spatial distance between subband states

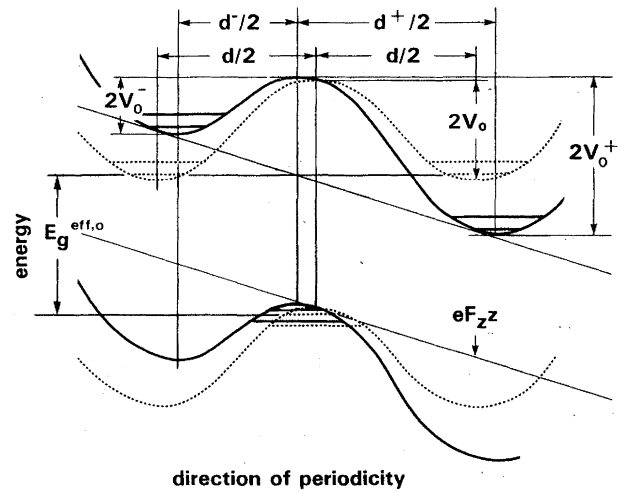


FIG. 5.  $n$ - $i$ - $p$ - $i$  crystal with an electric field  $F_z$  applied normal to the layers. The effective band gap and, therefore, the threshold energy for absorption is lowered. The subband spacings remain unaffected.

in adjacent layers, however, changes drastically. Therefore, the field  $F_z$  strongly influences the absorption coefficient  $\alpha^{n-i-p-i}(\omega; E_g^{\text{eff},0}, F_z)$ . Inspection of Fig. 5 and some elementary algebra tell us that the absorption coefficient can be calculated in the same manner as before. Evaluating expression (28) for  $\epsilon_2^{n-i-p-i}(\omega; E_g^{\text{eff},0})$ , one has only to replace it by one-half of the sum of two analogous contributions, obtained by substituting for  $2V_0$  and  $d$  by

$$2V_0 \rightarrow \begin{cases} 2V_0^+ = 2V_0(d^+) \\ 2V_0^- = 2V_0(d^-) \end{cases} \quad (54)$$

and

$$|\langle c, \mu | v, \nu \rangle^+|^2 \simeq |\langle c, \mu | v, \nu \rangle|^2 (1 + |F_z|/F_{\text{max}})^{2(\mu+\nu)} \exp[(-1/8)(d/\alpha)^2 (|F_z|/F_{\text{max}})(|F_z|/F_{\text{max}} + 2)] \quad (56)$$

and

$$|\langle c, \nu | v, \nu \rangle^-|^2 \simeq |\langle c, \mu | v, \nu \rangle|^2 (1 - |F_z|/F_{\text{max}})^{2(\mu+\nu)} \exp[(-1/8)(d/\alpha)^2 (|F_z|/F_{\text{max}})(|F_z|/F_{\text{max}} - 2)]. \quad (57)$$

Consequently, the increase of the transition probabilities according to (57) (or to the adjacent  $n$ -type layer on the left-hand side in Fig. 5) overcompensates for the decrease following from Eq. (56) (for transitions to the neighboring  $n$ -type layer on the right-hand side in Fig. 5). Thus, an overall increase of  $\alpha^{n-i-p-i}(\omega; E_g^{\text{eff},0}, F_z)$  according to

$$\alpha^{n-i-p-i}(\omega; E_g^{\text{eff},0}, F_z) \simeq \cosh[(d^2/8\alpha^2)(2|F_z|/F_{\text{max}})] \exp(-d^2 F_z^2 / 8\alpha^2 F_{\text{max}}^2) \quad (58)$$

results from the field-induced changes of the effective layer thicknesses.

The second effect of  $F_z$  concerns the splitting of the energy separation between conduction and valence subbands,

$$E_{\mu\nu}^0 = E_{c\mu} - E_{v\nu} = E_g^0 - 2V_0 + \hbar\omega_0(\mu + \nu + 1), \quad (59)$$

into two sets,  $E_{\mu\nu}^+$  and  $E_{\mu\nu}^-$ ,

$$E_{\mu\nu}^+ = E_{\mu\nu}^0 - 2V_0(2|F_z|/F_{\text{max}} + F_z^2/F_{\text{max}}^2) \quad (60)$$

and

$$E_{\mu\nu}^- = E_{\mu\nu}^0 + 2V_0(2|F_z|/F_{\text{max}} - F_z^2/F_{\text{max}}^2). \quad (61)$$

This splitting lowers the threshold for  $(\mu\nu)^+$  transitions at a given photon energy if  $F_z$  increases, which results in (strong) steplike increases of  $\alpha^{n-i-p-i}(\omega; E_g^{\text{eff},0}, F_z)$  each time the condition

$$E_{\mu\nu}^+(F_z) = \hbar\omega \quad (62)$$

is fulfilled. Similarly, a steplike decrease of  $\alpha^{n-i-p-i}(\omega; E_g^{\text{eff},0}, F_z)$  is expected if, with increasing  $F_z$ , the condition

$$E_{\mu\nu}^-(F_z) = \hbar\omega \quad (63)$$

is met.

In order to illustrate this rather complicated field dependence of the absorption coefficient, the situation is depicted in Figs. 6 and 7 for a simple situation where  $\hbar\omega$  is chosen such that only the lowest two conduction and valence subbands are participating in absorption processes at  $F_z=0$ . The design parameters ( $d=50$  nm,  $n_D=1.5 \times 10^{18}$  cm $^{-3}$ , and  $n_D/n_A=d_p/d_n=m_c/m_{LH}$ ) were determined such that  $\hbar\omega_c = \hbar\omega_{LH} \simeq 50$  meV and  $2V_0 \simeq 400$  meV. In Fig. 6 the valence-subband-con-

$$d \rightarrow \begin{cases} d^+ = d(1 + |F_z|/F_{\text{max}}) \\ d^- = d(1 - |F_z|/F_{\text{max}}). \end{cases} \quad (55)$$

The potential amplitudes  $V_0(d^+)$  and  $V_0(d^-)$  are calculated according to Eq. (3) with the new effective superlattice periods  $d^+$  and  $d^-$ , respectively.  $F_{\text{max}}$  is the ground-state maximum space-charge field at the interface between  $n$  and  $p$  layers, given by Eq. (51). From Eqs. (54) and (55) we see that the effect of  $F_z$  on the absorption will be twofold.

The field dependence of  $d^+$  and  $d^-$  results in strong superlinear changes of the transition probabilities. From Eqs. (33) and (37) we find, for  $\alpha_c = \alpha_v = \alpha$ ,

duction-subband separations  $E_{\mu\nu}^+$  and  $E_{\mu\nu}^-$  as a function of  $F_z$  are indicated by solid lines for  $E_{\mu\nu}^+(F_z)$  and  $E_{\mu\nu}^-(F_z) < \hbar\omega$ , i.e., for the region where transitions occur,

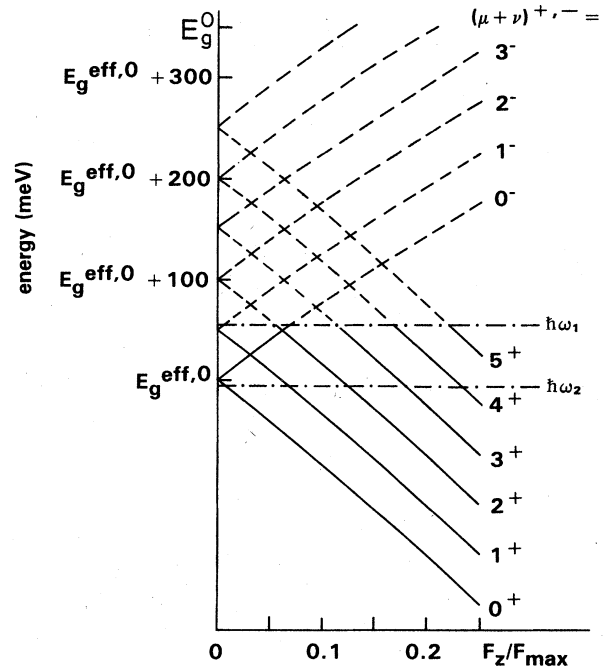


FIG. 6. Effective band gaps  $E_{\mu\nu}^+$  and  $E_{\mu\nu}^-$  as defined in Eqs. (61) and (62) for transitions between the  $\nu$ th valence and the  $\mu$ th conduction subbands to the left and the right neighboring layers as a function of the field  $F_z$ . Absorption is possible only for intersubband gaps  $E_{\mu\nu}$  smaller than the photon energy (see dashed-dotted lines labeled  $\hbar\omega_1$  and  $\hbar\omega_2$ ).

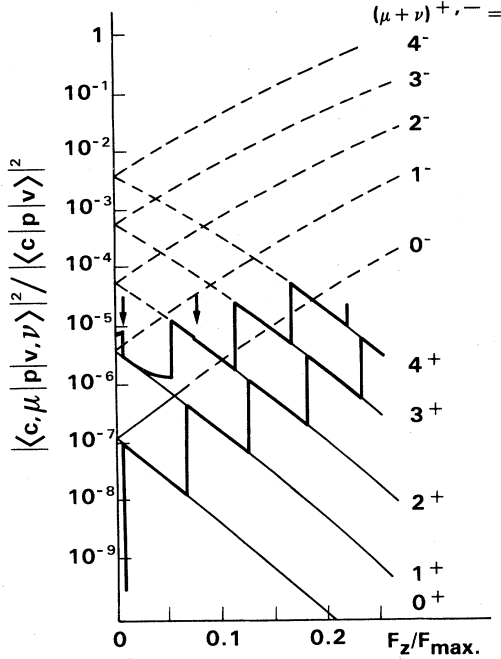


FIG. 7. Transition probabilities between different valence and conduction subbands  $\nu$  and  $\mu$  as a function of field  $F_z$ . The bold lines represent the sum of all allowed transitions at the photon energies indicated in Fig. 5. They reflect directly the field dependence of the absorption coefficient.

and by dashed lines above the photon energy. In Fig. 7 the squared interband matrix elements  $\langle c, \mu | \vec{p} | v, \nu \rangle^+$  and  $\langle c, \mu | \vec{p} | v, \nu \rangle^-$  are shown as a function of  $F_z$ . Again, the solid lines indicate the range where these matrix elements contribute to the absorption coefficient at the given photon energy. The bold line displays the sum of all contributions, i.e., the total absorption coefficient (see scale on the right-hand side of the figure). At low values of  $F_z$  we observe two steplike decreases, marked by arrows, associated with the cutoff for the  $\mu + \nu = 1$  and

$\mu + \nu = 0$  transitions to the left. The steplike increases result from transitions with  $\mu + \nu = 2, 3, 4$ , and 5, respectively, coming in with increasing field  $F_z$ . We also note a considerable increase of the absorption coefficient which is superimposed on the sawtooth-shaped oscillations of  $\alpha^{n-i-p-i}(\omega; E_g^{\text{eff},0}; F_z)$ . It is also worthwhile to mention that these oscillations occur at rather low values of  $F_z$  ( $F_{\max}$  is only about  $3 \times 10^5 \text{ V cm}^{-1}$  for our present example). Such fields can be created by the built-in voltage in an  $n-i-p-i$  structure of about 10 periods, sandwiched between an  $n$ -bottom and  $p$ -top layer, or vice versa. This means that very small external voltages are required in order to induce large relative changes of the absorption coefficient.

### B. Absorption in the excited state

The low recombination probability of photoexcited carriers in doping superlattices implies that the system will usually be in a metastable excited state even at low light intensities and/or low values of the absorption coefficient. The crystal then contains a finite number of electrons in the  $n$  layers and holes in the  $p$  layers whose distribution can be characterized by (different) quasi-Fermi levels  $\phi_n$  and  $\phi_p$ . The presence of charge carriers has two striking consequences for optical absorption.

(1) The superlattice potential, and therefore the effective band gap and the subband structure, will be different from the one in the ground state due to the partial compensation of the built-in impurity space charge by the electrons and holes. This has been discussed in great detail in the context of self-consistent subband-structure calculations for GaAs-doping superlattices in Ref. 14. For  $n-i-p-i$  structures in IV-VI materials it should be remarked that a much larger number of charge carriers than in GaAs is required to induce a significant change in the superlattice potential because of the large static dielectric constant of the host lattice.

(2) The partial occupation of subbands causes a Burstein shift in the absorption edge. The absorption threshold will no longer be given by Eq. (27), but by

$$\hbar\omega^{\text{th}} = \min_{i,j} \{ E_{c,\mu}^{(i)} - E_{v,\nu}^{(j)} + (\hbar^2/2) \max_{i,j} ((k_{f,\mu}^{(i)})^2, (k_{f,\nu}^{(j)})^2) [(m_c^{(i)})_{xy}^{-1} + (m_v^{(j)})_{xy}^{-1}] \}, \quad (64)$$

provided the transition  $|v, (j), \nu\rangle \rightarrow |c, (i), \mu\rangle$  is allowed and the  $k$ -selection rule applies strictly for the momentum  $\hbar\vec{k}_{\parallel}$  of carriers in these subbands. Here,  $k_{f,\mu}^{(i)}$  and  $k_{f,\nu}^{(j)}$  are the quasi-Fermi wave vectors for electrons and holes, respectively. The Burstein shift in GaAs-doping superlattices is more important than in bulk material because even a relatively low excitation intensity can induce a large concentration of photoexcited carriers and, therefore, large quasi-Fermi wave vectors. Furthermore, the fact that transitions from the light-mass valence bands dominate the absorption enhances the Burstein shift over that observed in the bulk, where the transitions from the heavy-mass valence band dominate. The Burstein shift also implies that the lowest transition is not necessarily the one between the lowest conduction and valence subbands.

We have used the results of self-consistent subband-structure calculations for GaAs-doping superlattices<sup>14</sup> to calculate the absorption coefficient for various excitation levels. As design parameters we selected  $n_D = 4 \times 10^{18} \text{ cm}^{-3}$ ,  $n_A = (m_{\text{LH}}/m_c)n_D$ , and  $d = 40 \text{ nm}$ . The results are shown in Figs. 8–12. Obviously, the absorption coefficient changes in magnitude and, in particular, in its frequency dependence as a function of carrier concentration.

In Fig. 13 we have plotted the absorption coefficient for a fixed photon energy as a function of the excitation level for the same GaAs  $n-i-p-i$  crystal. It should be noted that some of the steps in the absorption coefficient correspond to changes by almost an order of magnitude. Since the charge carriers may simply be produced by photoexcitation their concentration will be related to the intensity of the absorbed light. Therefore, the absorption in doping

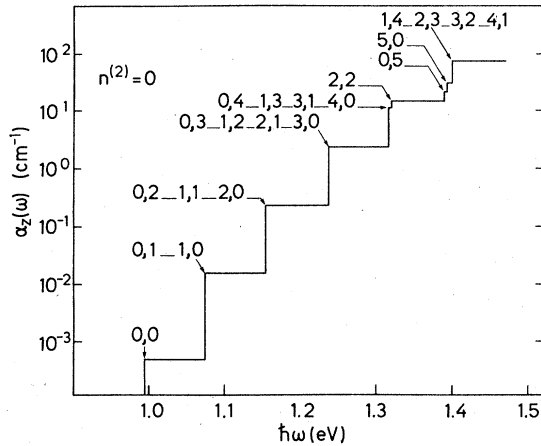


FIG. 8. Absorption coefficient of a compensated GaAs *n-i-p-i* crystal with  $n_D = 4 \times 10^{18} \text{ cm}^{-3}$ ,  $n_A = (m_{LH}/m_c)n_D$ , and  $d = 40 \text{ nm}$  at different nonequilibrium carrier concentrations, calculated numerically. The numbers indicate the valence- and conduction-band indices of transitions becoming allowed at a given photon energy. The absorption coefficient for  $\mu + \nu \leq 3$  has also been calculated analytically for the carrier-free ground state. The deviations from the numerical results are too small to be shown in the plot. At higher subband indices deviations from the harmonic-oscillator energies become apparent. The heavy-hole contributions are neglected in this example.  $n^{(2)} = 0$ .

superlattices is strongly intensity dependent, i.e., nonlinear. The discussion of the excitation kinetics and their consequences for low-intensity nonlinear phenomena is deferred to a planned subsequent publication.

#### IV. CONCLUSIONS

In this paper we have presented the theory of optical absorption in *n-i-p-i* doping superlattices together with the results of analytical and numerical calculations of the absorption coefficient  $\alpha(\omega)$ . We have found a pronounced steplike structure of the absorption coefficient as a function of photon energy which can extend far below the

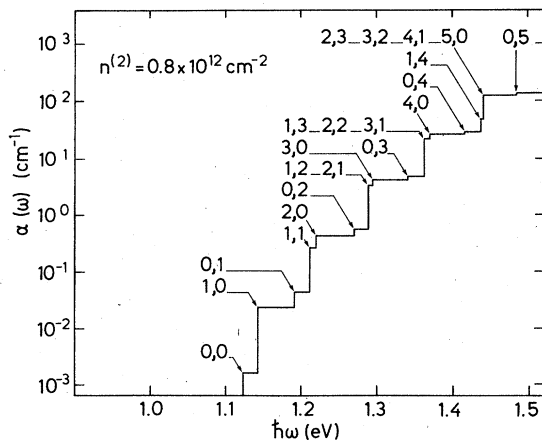


FIG. 9. Same as Fig. 8, except  $n^{(2)} = 0.8 \times 10^{12} \text{ cm}^{-2}$ .

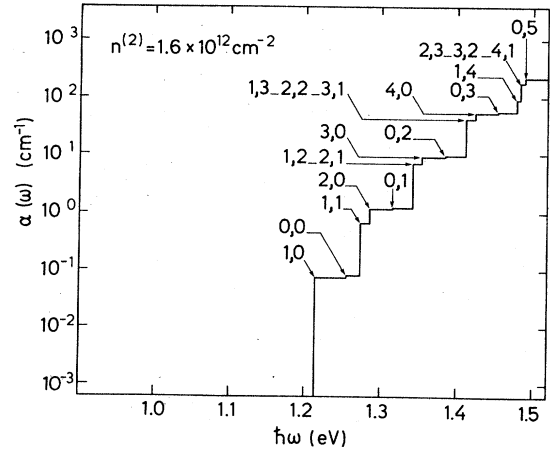


FIG. 10. Same as Fig. 8, except  $n^{(2)} = 1.6 \times 10^{12} \text{ cm}^{-2}$ .

band gap of the host material of the *n-i-p-i* structure. The strength of absorption for a given photon energy, and the threshold energy at which the absorption becomes zero, can be modulated for a given specimen within wide limits by the application of external fields normal to the layers of the superlattice or by changing the nonequilibrium carrier concentration.

We have tried to demonstrate the wide range of situations which can be encountered, depending on the choice of host material and design parameters. We have neglected a number of physical mechanisms which may affect the observed behavior in real *n-i-p-i* crystals, depending on the host material, the design parameters, and the photon energy. None of them, however, is expected to make the observation of any of the phenomena discussed in the present paper impossible.

The potential fluctuations, for instance, which result from the random spatial distribution of the impurity atoms,<sup>14</sup> may broaden the expected steps of the absorption coefficient. This will be important if the fluctuations are not screened by (a relatively small number of) charge carriers in the layers. The conditions for the observation of

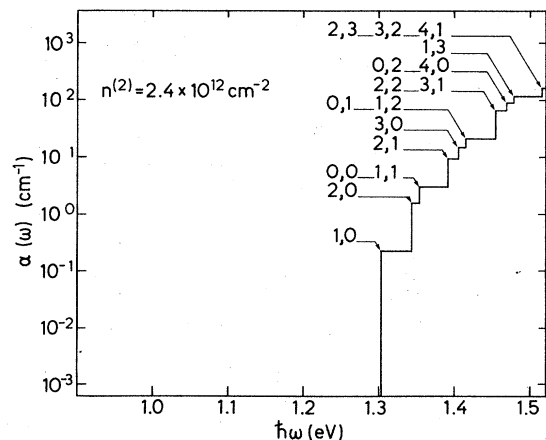


FIG. 11. Same as Fig. 8, except  $n^{(2)} = 2.4 \times 10^{12} \text{ cm}^{-2}$ .

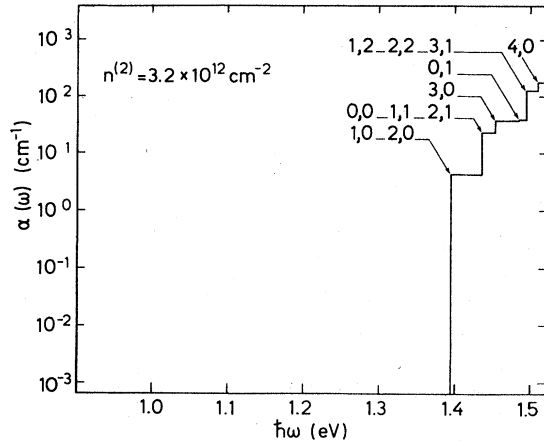


FIG. 12. Same as Fig. 8, except  $n^{(2)} = 3.2 \times 10^{12} \text{ cm}^{-2}$ .

the quantum structure in the absorption coefficient generally will be more favorable at high doping levels since the subband spacing increases faster than the potential fluctuations with increasing doping concentration. Moreover, a lower-band-gap material, such as InAs, will be more suitable than GaAs because of the larger subband spacing resulting from smaller electron and light-hole masses. *n-i-p-i* structures grown in IV-VI compounds, finally, seem ideal from the point of view of neglecting potential fluctuations and problems associated with impurity-band formation (see Refs. 14 and 20) because of their large static dielectric constant which makes the potential fluctuations small and prevents the formation of impurity bands.

The effective-mass approximation, which has been used throughout this paper, on the other hand, will become unsatisfactory more often in the lower-band-gap materials. The subband spacing will be overestimated because of the neglected nonparabolicity at higher subband indices. The matrix elements, on the other hand, will be underestimated because of the errors introduced by the EMA calculation for the overlap between conduction- and valence-subband envelope wave functions.

We have not considered in detail the consequences of our results for the observation of peculiarities in the photoconductive response, of nonlinearities in the absorption coefficient, for optical gain, or for the generation of spin-polarized electrons, nor have we discussed device applications of these unusual properties.

We should also point out that the choice of design pa-

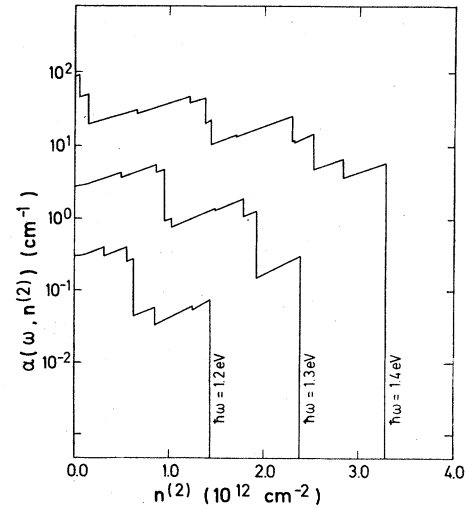


FIG. 13. Absorption coefficient as a function of carrier concentration for the photon energies indicated for the same example as in Fig. 8.

rameters for the examples presented in this study was not made aiming for favorable conditions for device applications. The appropriate design for devices depends on their purpose. For ultrafast modulation of the absorption coefficient at given photon energy by a field  $F_z$  in an electro-optical modulator, e.g., see Sec. III A, the optimized design is achieved by high doping levels and small superlattice period. Such a configuration will combine a sharp increase of  $\alpha$  values from close to 0 up to  $10^1$ – $10^3 \text{ cm}^{-1}$  at the given photon energy  $\hbar\omega \leq E_g^{\text{eff},0}$  under low values of  $F_z$  and with recombination lifetimes which are sufficiently short to prevent a signal-dependent "floating" of the absorption edge. If, on the other hand, a sensitive photoconductive detector working quite far below the gap of the host material is to be designed, a device with  $E_g^{\text{eff},0} \ll E_g^0$  provides a wide absorption tail. Long carrier-recombination lifetimes are obtained by moderate doping and a large superlattice period. While an adequate description for the former case is only provided by our present theory, the latter case can be treated with our semiclassical theory.<sup>11</sup> In fact, the latter case is more appropriate, not only from the point of view of requiring much less computational effort, but also on theoretical grounds. In cases where  $E_g^{\text{eff},0} \simeq 0$ , the absorption for photon energies not far below the gap of the host material,  $E_g^0$ , involves transitions between high-index subbands, to which the EMA can no longer be applied.

\*On leave of absence at Hewlett-Packard Laboratories, 1501 Page Mill Road, Palo Alto, CA 94603.

†Present address: Code 6877, Naval Research Laboratory, Department of the Navy, Washington, D.C. 20375.

<sup>1</sup>G. H. Döhler, Phys. Status Solidi B 52, 79 (1972); 52, 533 (1972).

<sup>2</sup>G. H. Döhler, J. Vac. Sci. Technol. 16, 851 (1979).

<sup>3</sup>G. H. Döhler, in *Festkörperprobleme: Advances in Solid State Physics*, edited by P. Grosse (Vieweg, Braunschweig, 1983), Vol. XXIII, p. 207.

<sup>4</sup>G. H. Döhler, Jpn. J. Appl. Phys. Suppl. 22, 29 (1983).

<sup>5</sup>R. Dingle, in *Festkörperprobleme: Advances in Solid State Physics*, edited by H. J. Queisser (Vieweg, Braunschweig, 1975), Vol. XV, p. 21.

<sup>6</sup>L. Esaki, J. Cryst. Growth, 52, 227 (1981).

<sup>7</sup>G. H. Döhler, H. Künzel, D. Olego, K. Ploog, P. Ruden, H. J. Stolz, and G. Abstreiter, Phys. Rev. Lett. 47, 864 (1981).

<sup>8</sup>K. Ploog, H. Künzel, J. Knecht, A. Fischer, and G. H. Döhler, Appl. Phys. Lett. 38, 870 (1981).

<sup>9</sup>K. Ploog, H. Jung, H. Künzel, and P. Ruden, Jpn. J. Appl.

- Phys. Suppl. **22**, 287 (1983).
- <sup>10</sup>H. Jung, G. H. Döhler, H. Künzel, K. Ploog, P. Ruden, and H. J. Stolz, *Solid State Commun.* **43**, 291 (1982).
- <sup>11</sup>G. H. Döhler, H. Künzel, and K. Ploog, *Phys. Rev. B* **25**, 2616 (1982).
- <sup>12</sup>H. Künzel, G. H. Döhler, P. Ruden, and K. Ploog, *Appl. Phys. Lett.* **41**, 852 (1982).
- <sup>13</sup>H. Jung, G. H. Döhler, E. G. Göbel, and K. Ploog, *Appl. Phys. Lett.* **43**, 40 (1983).
- <sup>14</sup>P. Ruden and G. H. Döhler, *Phys. Rev. B* **27**, 3538 (1983).
- <sup>15</sup>K. Ploog, A. Fischer, and H. Künzel, *J. Electrochem. Soc.* **128**, 400 (1981).
- <sup>16</sup>P. Ruden and G. H. Döhler, *Phys. Rev. B* **27**, 3547 (1983).
- <sup>17</sup>H. M. Gibbs, S. S. Tarng, J. L. Jewell, D. A. Weinberger, K. Tai, A. C. Gossard, S. L. McCall, A. Passner, and W. Wiegmann, *Appl. Phys. Lett.* **41**, 221 (1982).
- <sup>18</sup>F. Stern and W. E. Howard, *Phys. Rev.* **163**, 816 (1967).
- <sup>19</sup>D. L. Mitchell and R. F. Wallis, *Phys. Rev.* **151**, 581 (1966).
- <sup>20</sup>D. H. Döhler and P. Ruden, *Surf. Sci.* (to be published).
- <sup>21</sup>E. O. Kane, in *Semiconductors and Semimetals*, edited by R. K. Willardson and A. C. Beer (Academic, New York, 1972), Vol. 1, p. 75.
- <sup>22</sup>G. Fishman and G. Lampel, *Phys. Rev. B* **16**, 820 (1977).
- <sup>23</sup>D. T. Pierce and F. Meier, *Phys. Rev. B* **13**, 5484 (1976).